

www.acsanm.org Article

Lectin-Modified Bacterial Cellulose Nanocrystals Decorated with Au Nanoparticles for Selective Detection of Bacteria Using Surface-**Enhanced Raman Scattering Coupled with Machine Learning**

Asifur Rahman, Seju Kang, Wei Wang, Qishen Huang, Inyoung Kim, and Peter J. Vikesland*



Cite This: ACS Appl. Nano Mater. 2022, 5, 259-268



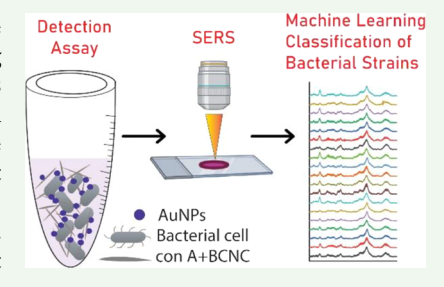
ACCESS I

Metrics & More

Article Recommendations

Supporting Information

ABSTRACT: Bacterial cellulose nanocrystals (BCNCs) are tunable and biocompatible cellulose nanomaterials that can be easily bioconjugated and used for biosensing applications. We report the application of concanavalin A (con A) lectin-modified BCNCs (con A + BCNCs) for bacterial isolation and label-free surface-enhanced Raman spectroscopy (SERS) detection of bacterial species using Au nanoparticles (AuNPs). The aggregated AuNP + bacteria + (con A + BCNC) conjugates generated SERS hot spots that enabled the SERS detection of the strain Escherichia coli 8739 at the 10³ CFU/mL level. The optimized detection assay was then used to differentiate 19 common bacterial strains. The large SERS spectral dataset for the 19 bacterial strains was analyzed using the support vector machine (SVM), an optimization-based machine-learning technique that worked as



a binary classifier. The SVM classifier showed a high overall accuracy of 87.7% in correctly discriminating bacterial strains. This study illustrates the potential of combining low-cost nanocellulose-based SERS biosensors with machine-learning techniques for the analysis of large spectral datasets.

KEYWORDS: lectin, cellulose, classification, surface-enhanced Raman scattering (SERS), bacteria, support vector machine (SVM)

■ INTRODUCTION

The global spread of antimicrobial-resistant microorganisms is considered a pressing threat to humankind in the 21st century.^{1,2} In particular, rapid detection and identification of pathogenic bacteria remain critical challenges to overcome if we are to minimize the spread of infectious diseases and protect public health.³ The conventional methods for bacterial detection are culture-based colony counting, polymerase chain reaction (PCR), and enzyme-linked immunosorbent assays (ELISA). While these methods have a proven track record for reliable, accurate, and sensitive pathogen detection, they require specialized equipment and trained personnel and are often expensive and time-consuming. Alternative biosensing techniques with rapid, reliable, and cost-effective detection are highly desired.

Surface-enhanced Raman spectroscopy (SERS) is a widely explored biosensing technique for rapid and cost-effective detection of microorganisms. SERS reflects the enhanced inelastic scattering of molecules associated with the surfaces of plasmonic gold (Au) or silver (Ag) nanoparticles. Depending on the composition of the analyte or the substrate, SERS enhancement factors of up to 1014 relative to conventional Raman have been reported.⁶ SERS is widely used for biosensing because of its low detection limits and for its relatively simple implementation.^{7,8} The continuous development of SERS substrates has enabled a range of SERS-based approaches to biosensing, including paper-based, liquid,

microfluidic, magnetic separation-induced, and electrochemical SERS.5

SERS bionanosensors of various types have been previously used for the detection of bacterial pathogens. ⁹ Zhang et al. used antibody-functionalized Au-coated magnetic nanoparticles (AuMNPs) for Staphylococcus aureus capture and separation. 10 Au nanorods (AuNRs) functionalized with the SERS tag 5,5-dithio-bis-(2-nitrobenzoic acid) and S. aureus antibodies were used for specific recognition and detection at a 10 cell/mL detection limit. 10 A similar sandwich-structured detection assay was employed by Kearns et al., where they used lectin-functionalized MNPs for the capture and isolation of three different antimicrobial-resistant bacteria.⁴ The isolated bacteria were detected at a concentration of 10 colony-forming units per mL (CFU/mL) using SERS-active AgNPs functionalized with strain-specific antibodies.⁴ More recently, Tadesse et al. used a controlled liquid chamber in a silica substrate for identification and drug susceptibility testing of viable bacteria cells.11

Received: September 2, 2021 Accepted: December 22, 2021 Published: January 7, 2022





In this study, we used concanavalin A (con A) lectinfunctionalized bacterial cellulose nanocrystals (con A + BCNCs) for specific binding to and isolation of bacterial cells. AuNPs were then immobilized onto the bacteria + (con A + BCNC) conjugates for label-free SERS detection of bacteria. Cellulose paper-based SERS substrates are often incorporated with plasmonic Ag or AuNPs for rapid and lowcost analyte detection. 12,13 In our previous work, AuNPs were incorporated into bulk bacterial cellulose (BC), and the resulting AuNP + BC nanocomposites were used as SERS substrates. 14 More recently, we functionalized BCNCs with iron oxide (Fe₃O₄) and AuNPs to develop hybrid nanocomposites for magnetic separation and SERS detection. ¹⁵ To date, a majority of the cellulose paper-based SERS substrates described in the literature have been bulk substrates. 16-18 Notably, however, BCNCs produced by strong acid hydrolysis of bulk BC are colloidally and thermally stable in micro- and nano-dispersions, while retaining the high specific surface area and tensile strength of cellulose materials. 15,20

Lectins are a large family of proteins that can specifically bind to carbohydrate components on the surface of bacterial cell walls. Con A, a legume sourced lectin, has high affinity for the D-mannose and α -glucose functional groups on all bacterial surfaces. Using a SERS droplet microfluidics platform, we previously reported on the use of wheat germ agglutin (WGA) lectin-functionalized AuNPs for the elucidation of glycan expression on the surface of prostate cancer cells. Lectin-based biosensors have been widely used for the detection of pathogenic bacteria because of their specific binding capability and their stability. Lectin-based biosensors have been widely used for the detection of pathogenic bacteria because of their specific binding capability and their stability.

While the SERS spectrum for a bacterial strain may reflect a unique fingerprint, the similarities of the SERS profiles of different bacterial strains pose challenges for label-free discrimination. Conventional peak ratio comparisons of bacterial SERS profiles are often inadequate when analyzing features from large SERS datasets. However, machine-learning and deep-learning techniques are well-suited to analyze correlations and predict features within such datasets.²⁵⁻²⁸ The support vector machine (SVM) is an optimization-based machine-learning technique that works as a discriminative classifier to separate high-dimensional data using a hyperplane.²⁹ Through iterative weighting of data points, known as support vectors, the distance between the different classes (i.e., different bacterial strains) is maximized by the separating hyperplane.³⁰ The SVM is robust enough to handle complex datasets, where classes are not linearly separable. The visualization of the hyperplane using different kernel functions (e.g., linear, polynomial, and Gaussian) as classifiers allows for the discrimination and accurate prediction of features in complex datasets. The detailed procedure for kernel optimization can be found in the literature on SVM techniques. 30,31 Previously, Kusić et al. combined Raman spectroscopy and SVM to discriminate Legionella and other aquatic bacteria with an overall ~88% prediction accuracy.³² Recently, Kang et al. developed a tool that combined a treebased decision rule with SVM (Tr-SVM) for the discrimination of single-strand DNA gene sequences based on their SERS spectra.

The (con A + BCNCs) developed in this study were incubated with suspended bacterial cells. The isolated and aggregated bacteria + (con A + BCNC) conjugates were then treated with AuNPs for SERS interrogation. We collected SERS spectra of 19 bacterial strains to test the versatility of the

SERS substrate and to apply the SVM model for the discrimination and classification of bacterial strains.

EXPERIMENTAL SECTION

A detailed description of the chemicals used is provided in the Supporting Information. The AuNPs used in this study were prepared using methods previously described by Brown et al. and are described in the Supporting Information.³⁴

Bacterial Strains and Growth Conditions. The 19 bacterial strains from 10 different bacterial species used herein are listed in Table S1. Detailed descriptions of the growth conditions and protocols used to prepare bacterial stock solutions are provided in the Supporting Information. The different growth conditions for different strains were used for optimal growth of the strains according to the ATCC propagation procedure for each. The bacteria stock solutions used for the detection experiments had an optical density $(\mathrm{OD}_{600\mathrm{nm}})$ in the range of 0.6-0.8 ($\sim 10^8$ CFU/mL).

Synthesis and Surface Modification of BCNCs. The bulk BC and the BCNCs used in this study were synthesized according to previously published methods from our group and are described in detail in the Supporting Information. 14,15 Prior to lectin modification, the BCNC surface was -COOH functionalized via (2,2,6,6-tetramethylpiperidin-1-yl)oxyl or (2,2,6,6-tetramethylpiperidin-1-yl)oxidany (TEMPO)-mediated oxidation. 35 Briefly, 1 g of BCNCs (wet wt.) was suspended in 0.05 M of PBS buffer (90 mL, pH \sim 7) containing TEMPO (0.016 g, 0.1 mmol) and NaClO2 (80%, 1.13 g, 10 mmol) in a sealed round-bottom flask. Then, 0.1 M of NaOCl (0.5 mL) in 1× PBS was quickly added using a syringe. The suspension was magnetically stirred at 450 rpm and 120 °C for 24 h. Afterward, the suspension was cooled to room temperature, and the TEMPO-oxidized BCNCs were washed 3× with deionized (DI) water and resuspended in 50 mL of DI water until use.

Lectin modification was performed using EDC/NHS (N-ethyl-N'-(3-(dimethylamino)propyl)carbodiimide/N-hydroxysuccinimide) cross-linking chemistry. 4,36,37 A 2 mL aliquot of the TEMPO-oxidized BCNCs in a microcentrifuge tube was centrifuged at 22,150 ×g for 30 min. The supernatant was decanted, and the BCNCs were resuspended in 1 mL of 50 mM MES (2-[morpholino]ethanesulfonic acid) coupling buffer containing EDC (24 μ L, 200 mM in DI water) and NHS (120 μ L, 200 mM in MES buffer). MES is preferred as a buffer at pH 6 for activation reactions using EDC/NHS.³⁶ The EDC and NHS solutions were prepared beforehand and mixed together before being added into the BCNC suspension. The conjugates were shaken for 1 h at room temperature, centrifuged again, and then resuspended in 1 mL of HEPES (4-(2-hydroxyethyl)-1-piperazineethanesulfonic acid) buffer containing 0.2 mg/L of con A. The asproduced conjugates were shaken overnight. Following mixing, the conjugates were centrifuged, and the lectin-modified BCNCs were suspended in 0.01 M PBS (1x).

Detection Assay and the Limit of Detection. For each of the 19 bacterial strains, 100 μ L of bacterial stock solution was added into 500 μ L of the lectin-modified BCNC suspension in 1× PBS. The mixture was shaken for 40-50 min, followed by a brief centrifugation (9800 ×g, for 1 min) for rapid separation of the aggregated conjugates. The supernatant was removed and 200 µL of AuNPs (~ 0.1 nM) was added to resuspend the conjugates. The amount of AuNPs optimized for 500 µL of BCNCs may need adjustment, depending on the amount of BCNCs. Following 5 min of exposure, the AuNPs were adsorbed onto the fibers of the BCNCs. The conjugates were aggregated using centrifugation (6300 ×g, for 3 min) and concentrated in 20 μ L of DI water. A 10 μ L droplet of the AuNPs + bacteria + (con A + BCNC) conjugates was dried on aluminum foil at 40 °C and used for SERS analysis. To calculate the limit of detection (LOD), the best-fit regression line was determined from the plot of the intensity ratio of the peaks (I_{730}/I_{77}) against the logarithm of E. coli 8739 concentrations.

$$I_{730}/I_{77} = a \log C + b$$

where a and b are the slope and y intercept of the regression line, respectively. The LOD was calculated using the following equation,

$$\log LOD = (3\sigma_a - b)/a$$

where σ_a is the standard deviation of the slope of the regression line. Instrumentation. SERS spectra of the dried AuNPs + bacteria + (con A + BCNC) conjugates for each bacterial strain were collected using a WITec Alpha500R Raman Spectrometer with 785 nm laser excitation and a 10× confocal microscope objective lens. For each measurement, the laser power was adjusted to ~3.2 mW, with the spectral center set to 1500 cm⁻¹ and an acquisition time of 1 s. The peak intensities were obtained by measuring $20 \times 20 \ (X \times Y)$ points across a $100 \times 100 \ \mu\text{m}^2$ area using 1 s integration time per point. The automated peak labeling feature within the WITec Control Five (v. 5.0) software was used to select SERS peaks using a minimum relative height of 0.1. The data were baseline-corrected using an asymmetric least-squares smoothing (AsLS) method. Scanning electron microscopy characterization was performed using a field-emission scanning electron microscope (FESEM, LEO (Zeiss) 1550) operating at 5 kV with InLens detector mode. Ultraviolet-visible (UV-vis) measurements were performed using a Cary 5000 UV-vis-NIR spectrophotometer. A Zetasizer Nano ZS dynamic light scattering (DLS) instrument was used for zeta potential measurement.

Data Preprocessing and Model Development. We collected the SERS spectra of 19 different bacterial strains to build up a dataset for training, validation, and evaluation of the prediction capabilities of the SVM classifiers. For each bacterial measurement, $400 (20 \times 20)$ SERS spectra were collected using the large area scan method. For each spectra, cosmic spike removal, peak smoothing (Savitzky-Golay method), and baseline correction (AsLS method) were performed using the WITEC Control Five (v. 5.0) software. After preprocessing, 13 spectral features, labeled using the WITEC software, for the SERS peaks of interest between 600 and 1700 cm⁻¹ were extracted. To account for point-to-point variability, the extracted features were normalized using the peak at 1326 cm⁻¹ (excluded from the model development), corresponding to the ring vibration of adenine. 38,39 A total of 7600 spectra from 19 bacterial strains with 12 normalized spectral features were used to develop the discriminatory SVM classifier. To account for the heterogeneity of the SERS substrate and the variability induced by measurement intervals, five replicates of E. coli K12 as a representative strain were analyzed in five consecutive days, and the variability in the SERS profiles was analyzed.

To analyze the large SERS dataset and discriminate the 19 bacterial strains, a binary SVM classifier tool was trained using the classification learner application in Mathworks MATLAB/Simulink (ver. 2020a). Because SVM does not natively support multiclassification (hence, binary), the multiclass classification dataset (19 bacterial strains into 19 classes) was split into multiple binary classification datasets using two commonly used voting strategies: one vs one and one vs all. One vs one is a pairwise binarization approach using pairwise comparison between classes (E. coli K12 vs E. coli 8739, E. coli K12 vs E. coli 25,922, and so on). The one vs all strategy compares each class of dataset to the rest of the classes (E. coli K12 vs the rest, E. coli 8739 vs the rest, and so on). Following the training step, the performance of the classification model was evaluated using true-positive/-negative rates and false-positive/-negative rates. These indicators were reported in a confusion matrix that allows for the visualization of the model performance by summarizing the counts of the predicted and the actual classes. Using these indicators, the overall accuracy, sensitivity, and specificity of the SVM classifier were calculated. The overall accuracy indicates the proportion of the reference data that were mapped correctly. Sensitivity and specificity indicate the proportion of the correctly identified number of actual positives and actual negatives, respectively. The trained model was validated using 10-fold cross validation. To describe briefly, the dataset (7600 spectra) was divided into 10 subsets of equal size, 9 of which were used to train the model and 1 left out to test the model. This procedure was iterated until every subset was used for model testing. This iterative prediction procedure applied to unseen data by cross validation indicates the model's generalizability.

RESULTS AND DISCUSSION

Lectin-Modified BCNCs as SERS Substrates. The conjugation of bacteria and AuNPs onto the fibers of the BCNCs allowed us to develop a versatile SERS substrate along with a straightforward detection assay for SERS measurements (Figure 1). The use of con A allows for multivalent interactions

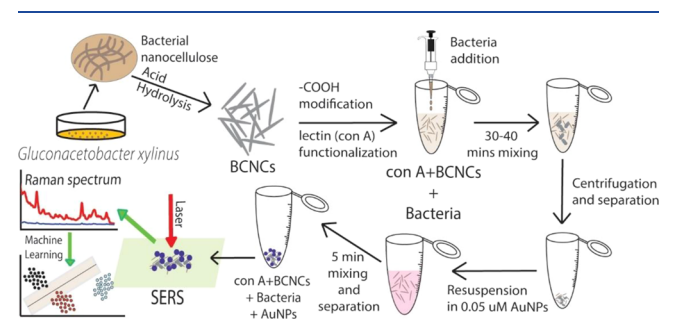


Figure 1. Schematic illustration of synthesis and functionalization of BCNCs, bacteria detection assay, SERS and machine-learning applications.

between (con A + BCNCs) and the sugar moieties of the bacterial cell surface. 4,41 The incubation of (con A + BCNCs) with bacterial strains leads to the aggregation of the conjugates, which can then be quickly separated via brief centrifugation. The negatively charged AuNPs (-34.1 ± 0.8 mV) were rapidly immobilized onto the neutral to positive (con A + BCNC) conjugates (2.44 \pm 1.6 mV), suggesting that the carboxylated BCNCs act as a support for AuNPs. 15,42 Compared to using only colloidal Au/Ag NPs as SERS substrates, the use of dispersible cellulose substrates enables greater control over AuNP aggregation in suspension and increased stability of aggregated AuNPs. 15,42,43

We compared the SERS spectra from two different bacterial strains: *E. coli* K12 and *P. syringae* in dried vs liquid state. The higher overall SERS intensity from the dried droplets compared to the liquid droplets suggested the close proximity of aggregated AuNPs produced localized SERS hot spots, resulting in increased SERS signals (Figure S2A). The presence of aggregated AuNPs on the bacteria + (con A + BCNC) conjugates resulted in an increase in the SERS peak intensity relative to the control with no bacteria (Figure S2B). After hot spot normalization, the peak intensities at 1326 cm⁻¹ were ~6× and ~2.5× higher for AuNPs + *E. coli* K12 + (con A + BCNCs) compared to the control with no bacteria and AuNPs + *E. coli* K12 only (Figure S2B).

SEM characterization of the aggregated, carboxylated BCNCs revealed a network of interwoven cellulose fibers (Figure 2A). Figure 2B shows isolated BCNCs consisting of rod- or needle-shaped structures of 400 nm-800 nm in length and 30-40 nm in width. SEM micrographs indicate the presence of con A on the surface of BCNCs, as highlighted in Figure 2C. Figure 2D shows the distribution of *E. coli* K12 cells on the surface of the (con A + BCNCs) in approximately a 100 $\mu m \times 100 \ \mu m^2$ area, equivalent to the Raman large area scan measurements for collecting SERS spectra for each bacterial strains. A SEM micrograph of a single E. coli K12 cell (Figure 2E) on aggregated con A + BCNCs suggests the partial coverage of BCNC fibers on the surface of bacteria. Upon the addition of AuNPs onto the BCNC fibers, AuNPs were observed on both the fibers and the bacterial surface, thus resulting in the AuNPs + bacteria + con A + BCNC conjugates

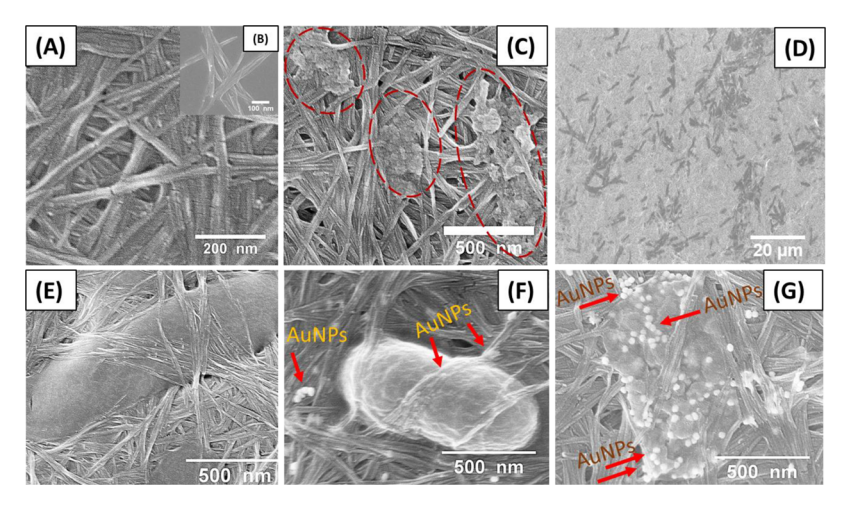


Figure 2. Scanning electron micrographs of (A) aggregated BCNCs. (B) A few isolated BCNCs(C) Con A lectin-functionalized BCNCs with the presence of lectin highlighted. (D) Overview image of the bacteria *E. coli* K12 in a $100 \times 100 \ \mu m^2$ area on the surface of (con A + BCNCs). (E) Scaled up image of a *E. coli* K12 on (con A + BCNCs). (F) Aggregated AuNPs + *E. coli* K12 + (con A + BCNCs) conjugate and (G) Aggregated AuNPs + *P. syringae* + (con A + BCNCs) conjugate.

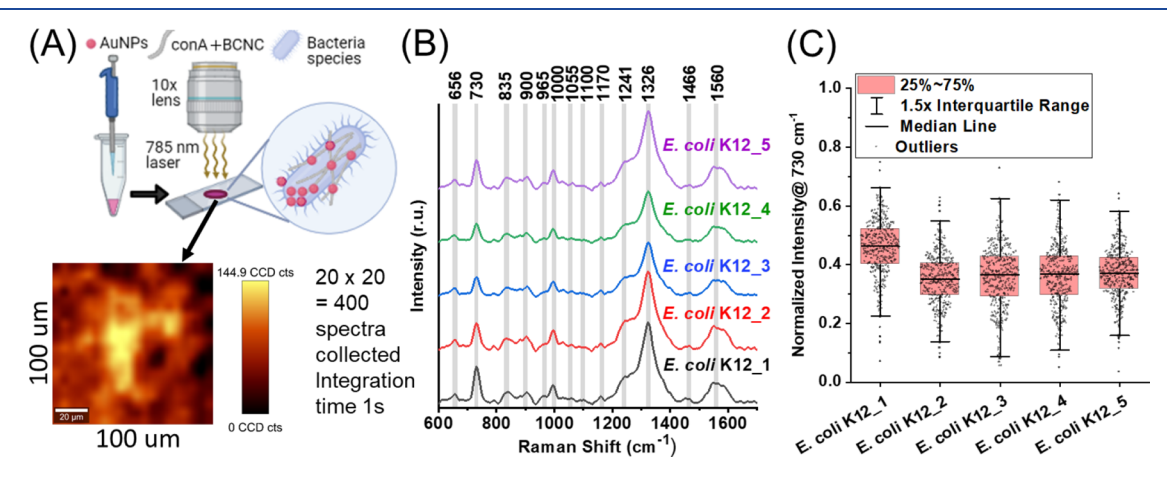


Figure 3. (A) Schematic illustration of the experimental setup for label-free SERS measurements of bacteria strains with a $100 \times 100 \ \mu\text{m}^2$ SERS map at 77 cm⁻¹ of the aggregated AuNPs-bacteria-(con A + BCNCs) substrate. (B) Average of 400 SERS spectra for five replicates of *E. coli* K12 bacteria (named *E. coli* K12_1 to *E. coli* K12_5), showing the 13 selected peaks (gray bars) on the spectra. (C) Boxplots with the distribution of data points for the hot spot-normalized peak intensity at 730 cm⁻¹ for five *E. coli* K12 replicates in this study.

used for the SERS measurement. Figure 2F,G shows the AuNPs + bacteria + (con A + BCNC) conjugates for *E. coli* K12 and *Pseudomonas syringae* (*P. syringae*). UV—vis measurements exhibit peak broadening and a decrease in absorbance when *E. coli* K12 and *P. syringae* were associated to AuNPs + (con A + BCNC) compared to the control (Figure S3). These results suggest the association of bacteria and AuNPs to (con A + BCNC), resulting in the SERS conjugates. This lectin detection assay was used for each of the 19 bacterial strains for SERS detection and development of the SERS dataset.

SERS Detection of Bacterial Strains. For each of the bacterial strains, $10 \mu L$ of the AuNP + bacteria + (con A + BCNC) conjugates in DI water were dried, and the dried droplet was analyzed using 785 nm laser excitation and a $10 \times$ objective lens (Figure 3A). Following solvent evaporation, AuNPs-bacteria-(con A + BCNCs) aggregates were observed using a Raman confocal microscope. As shown in the representative SERS map of $\sim 100 \times 100 \mu m^2$ area for the 77 cm⁻¹ position (Figure 3A, bottom), the ubiquitous presence of hot spots was observed across the substrate. The pseudoband at 77 cm⁻¹ reflects elastically scattered light, resulting

from the interaction of amplified spontaneous emission (ASE) of the incident laser and the Raman edge filter. 6,44 The variation of the pseudo-peak at 77 cm⁻¹ reflects the density of SERS hot spots and can be used for the normalization of hot spot variability. 6,44-46 The heterogenous arrangement of plasmonic nanostructures on the SERS substrate can result in point-to-point variability of SERS substrates in the measured SERS signals. To account for this spatial variability, we performed E. coli K12 identification experiments five times and reported the average of 400 spectra for all five replicates (Figure 3B). Figure 3C provides boxplots with the distribution of data points for the hot spot-normalized peak intensity at 730 cm-1 for all five E. coli K12 replicates. The coefficient of variation (CV) of the normalized intensity at 730 cm⁻¹ was 29.3% or less for all five replicates. Furthermore, the boxplots for the normalized peak intensity at 730 cm⁻¹ and the corresponding CV values for all 19 bacterial strains are presented in Figure S4 and show a CV of 35.6% or less across bacterial strains. These results suggest, when considering both intrastrain

and interstrain variability, the (con A + BCNC) substrate showed relatively lower spatial variability compared to many commercial substrates with >45% variability.⁴⁷ The heterogenous distribution of NPs remains a challenge, which induces variability in SERS measurements. The use of hotpot normalization techniques and chemicals as internal standards can substantially lower this variability. 6,15,44 To determine the LOD, the detection assay was performed for E. coli 8739 over the concentration ranges of $10^7 - 10^1$ CFU/mL (Figure S5A). Below 103 CFU/mL, the data points had responses comparable to the blank, and hence were omitted. The normalized I_{730} can be reasonably approximated as a linear function of the logarithm of the E. coli 8739 concentration. The two parameters were statistically correlated with an R-square value of 0.9725, and the experimental data were within the 95% prediction region (Figure S5B). Using this approach, the LOD was determined to be $\sim 1.5 \times 10^3$ CFU/mL from the empirical best-fit equation and the standard error of the regression. This LOD is comparable to previously reported LODs for label-free detection of bacteria, as shown in Table S2.

Several distinct peak features were observed in the 600–1700 cm $^{-1}$ region of the SERS spectra for all 19 bacterial strains (Figure S6). Strong features at 730, 1000, 1241, 1326, and 1560 cm $^{-1}$ were common across all strains, but the relative peak intensities differed slightly. A total of 13 spectral features were selected by applying automated peak labeling in WITec Control Five (v.5.0) software. The band assignments for these peaks were made based upon the prior bacterial SERS spectra literature and are presented in Table $1.^{32,38,39,48-50}$ SERS

Table 1. Tentative Band Assignments for the Peaks Identified in the SERS Spectra of Bacteria

SERS band/cm	tentative band assignments	ref
656	ring vibration of guanine	38
730	ring vibration of adenine	38
835	cytosine/uracil/tyrosine	32,39
900	tryptophan	32
965	polysaccharide (bacterial cell wall)	32
1000	ring vibration of phenylalanine	32,38
1055	amine/phosphate/FAD (flavin adenine dinucleotide)	48,49
1100	amides of proteins	38
1170	C-N stretching, amides, DNA, adenine	39,49
1241	amide III of protein	38,39
1326	ring vibration of adenine	38,39
1466	CH ₂ deformation of lipids, proteins, carbohydrates	38,39,49
1560	C-H bend, C=C stretching	49,50

features arising from bacterial cells primarily reflect poly-saccharides, phospholipids, proteins, and nucleic acids. The characteristic band at 656 cm⁻¹ is attributed to the aromatic ring breathing mode of the base nucleotide guanine, while the bands at 730 and 1326 cm⁻¹ are attributed to adenine ring breathing. Among the proteins, the ring vibrations of the essential amino acids cytosine/uracil/tyrosine, trypotophan, and phenylalanine contribute to the bands at 835, 900, and 1000 cm⁻¹, respectively. Amide (I, II, III) functional groups of proteins are reflected in the bands at 1100 and 1241 cm⁻¹. Among the proteins of the bacterial cell wall, polysaccharides, and phospholipids are assigned to the band

at 965 cm⁻¹.³² The band at 1055 cm⁻¹ has been attributed to amines, phosphates, and adenine derivatives, such as flavin adenine dinucleotide (FAD).⁴⁸ The bands at 1170, 1466, and 1560 cm⁻¹ can be attributed to vibrational stretching, bending, or deformation modes of several components, such as C–N, C–H, and C=C, and these modes can originate from amides, lipids, proteins, DNA, and carbohydrates (Table 1).^{38,39,49,50}

There is reported variability in the band positions for bacteria (Table 1). For example, polysaccharides in our study exhibited a band at 965 cm⁻¹, while Kusić et al. reported a polysaccharide band at 960 cm⁻¹, but no peak at 965 cm⁻¹.³² The peak intensity and positions of bacterial Raman spectra are affected to varying degrees by the growth media, sample preparation method, storage time, and temperature, as suggested previously. 51-53 For example, Chisanga et al. reported a range of 720-740 cm⁻¹ and 1320-1340 cm⁻¹ for the adenine ring vibration, reflecting the heterogeneity in bacteria detection assays, from sample preparation to identification, across the literature. ^{39,49,54,55} The growth media and growth conditions of all bacteria used in this study are listed in Table S1. To minimize potential artifacts from the growth media, all samples were centrifuged and the pellet resuspended in 1× PBS solution three times before final resuspension in 1× PBS prior to SERS detection experiments. Despite the differences in their growth conditions, the bacterial strains showed similarity in SERS peak profiles and peak positions, suggesting minimal interference from the growth media (Figure S7). Previously, Harz et al. applied SVM to differentiate between Staphylococcus species and strains grown under varying culture conditions and achieved high accuracy rates of 94.1% at the strain level and 97.6% at the species level. 56 Furthermore, bacteria release metabolites, compounds essential for their cellular functions, into the supernatant.⁵⁷ The different culture conditions for bacterial growth used in this study can cause bacteria to produce different metabolites. The release of bacterial metabolites is affected by the storage time, the temperature, and the chemical composition of the storage media. 38-60 All of the bacteria strains in this study were stored at 4 °C, following growth and analyzed within 24 h of growth to minimize the potential effects of bacterial metabolite production on the SERS spectra.⁶¹

Discrimination and Identification of Bacterial Strains Using the SVM Classifier. Although different bacterial strains are characterized using their unique molecular compositions, the similarities in their corresponding SERS spectra reflect the difficulty in discriminating strains. For highdimensional and correlated Raman/SERS datasets, conventional peak ratio analysis and the use of multivariate analysis tools, such as principal component analysis (PCA), is often inadequate when evaluating the prediction accuracy of feature classes. For example, Chen et al. encountered the overlap of two species when using PCA to discriminate five bacterial species, concluding that spectral interference from similar features could not be differentiated.⁶² Hoehse et al. reported that combining PCA with SVM improved accuracy when classifying features based on Raman spectroscopy datasets. 63 To analyze the high-dimensional SERS dataset in this study, we extracted all the labeled peaks from the SERS spectra for discrimination using a SVM classifier.

The SERS spectra of the 19 bacteria in this study are vertically stacked and are presented in Figure 4A. The peak positions were highly consistent with slight differences in peak intensities across bacterial strains. In Figure 4B, our sequential

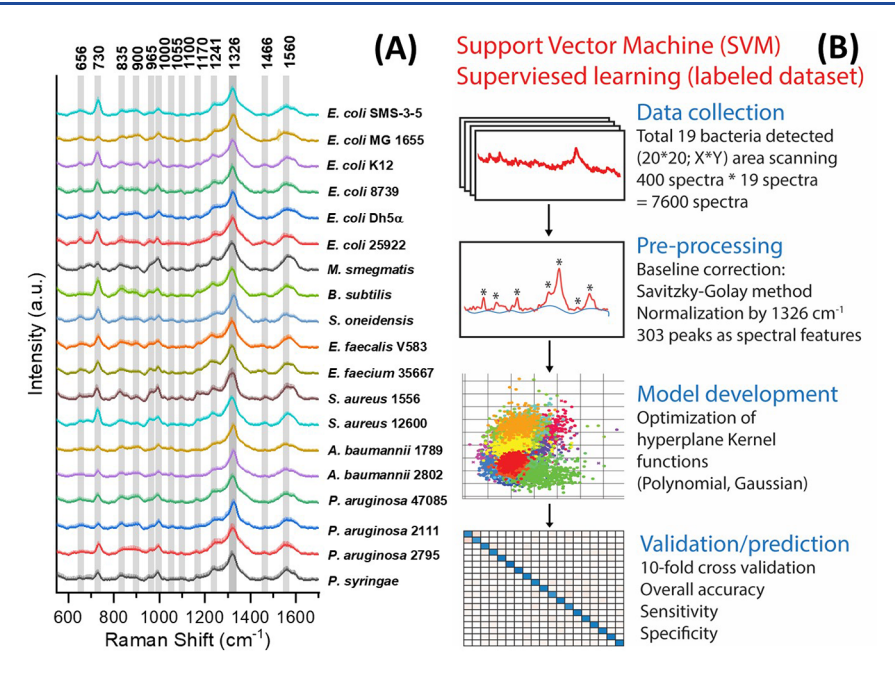


Figure 4. (A) Average of 400 SERS spectra with standard deviations for the 19 bacterial strains used in this study, normalized using the peak at 1326 cm⁻¹. (B) Schematic illustration showing the four major steps of developing the SVM predictive model: data collection, preprocessing, model development, and validation/prediction.

process going from SERS data collection to SVM model validation is shown. For each bacterial strain, all 400 spectra collected within the Raman large area scan were preprocessed (as described in the Experimental Section), and then the average spectra were calculated along with the standard deviation. The slightly different relative intensities of the 13 peaks, selected using the automated peak labeling feature and assigned band positions according to the previous literature, were used as features. Then, the peak at 1326 cm⁻¹ from the ring vibration of adenine (dark gray) was used to normalize the remaining 12 peaks. In Figure 4A, the normalized spectra containing the 12 normalized peak features (gray) were extracted to develop the SVM classifiers. In the model development stage, SVM computes a hyperplane that separates the classes of data points with the maximum margin (Figure 4B). A great advantage of the SVM is that when the classes are not linearly separable, data points can be projected to a higher dimensional space where they can be linearly separated, thus allowing the model to determine optimal hyperplanes in higher dimensional datasets.64

Herein, both polynomial (i.e., linear, quadratic, and cubic) and Gaussian (i.e., fine, medium, and coarse) kernel functions were used to classify features and find the best scoring algorithm. Interestingly, when PCA was preconducted, the number of useful features was reduced from 12 to 9, resulting in a decrease in the overall accuracy of the SVM models. Considering this outcome, we did not conduct PCA before running the models. All predictive models were validated using 10-fold cross validation.

In this study, peak selection was performed using the minimum relative height parameter of the automated peak labeling function in the WITec software, and the SERS bands were assigned according to the literature. This process resulted in 12-peak features in the range of 600–1700 cm⁻¹. When selecting peaks for the development of a predictive model, it is desirable to have a standardized procedure for determining spectral features that reflects all the possible variations in SERS

spectra, resulting from the varying compositions of macromolecules within the bacterial cells. However, indiscriminately selecting all spectral features, including baseline noise, for model development can result in a biased model. Such a model can be misleading because it fails to capture the trends in the dataset required for bacterial classification. In our dataset, considering the entire spectral range from 600 to 1700 cm⁻¹, a total of 302 spectral features were extracted at a resolution of ~4 cm⁻¹ (Figure S8A). PCA was preconducted to reduce the dimensionality of the dataset, which reduced the 302 features to 81 significant principal components (PCs) with an explained variance of ~95% (Figure S8B). The large number of PCs suggests that the SERS background and/or spectral noise are included in the peak intensities considered for training the model, and this may lead to model overfitting. During the preprocessing of the dataset, noise-level intensities can be processed differently, depending on the method of background correction, which can also bias the model. Hence, we opted for a standardized method (i.e., relative minimum height) for the selection of distinct peaks and assigned bands to those peaks according to the literature.

Different SVM classification models, along with linear and quadratic discriminant analysis (LDA and QDA) models were compared (Table S3). The overall accuracy scores of the models for the discrimination of the bacteria species followed the order: medium Gaussian SVM > quadratic SVM > cubic SVM≈QDA≈linear SVM > LDA > coarse Gaussian SVM > fine Gaussian SVM. The medium Gaussian SVM classifier with one vs one voting strategy was used for final reporting. Figure S9 shows the boxplots of 10 prediction results from the 10-fold cross validation for different models. For the bacterial dataset in this study, all the models were performed with statistically similar accuracies, except the fine Gaussian SVM (Wilcoxon signed ranked test, $\alpha = 0.05$) (Table S4). For both the one vs one and one vs all voting strategies, the medium Gaussian kernel achieved the highest overall accuracy among all SVM classifiers when discriminating bacterial strains from the SERS

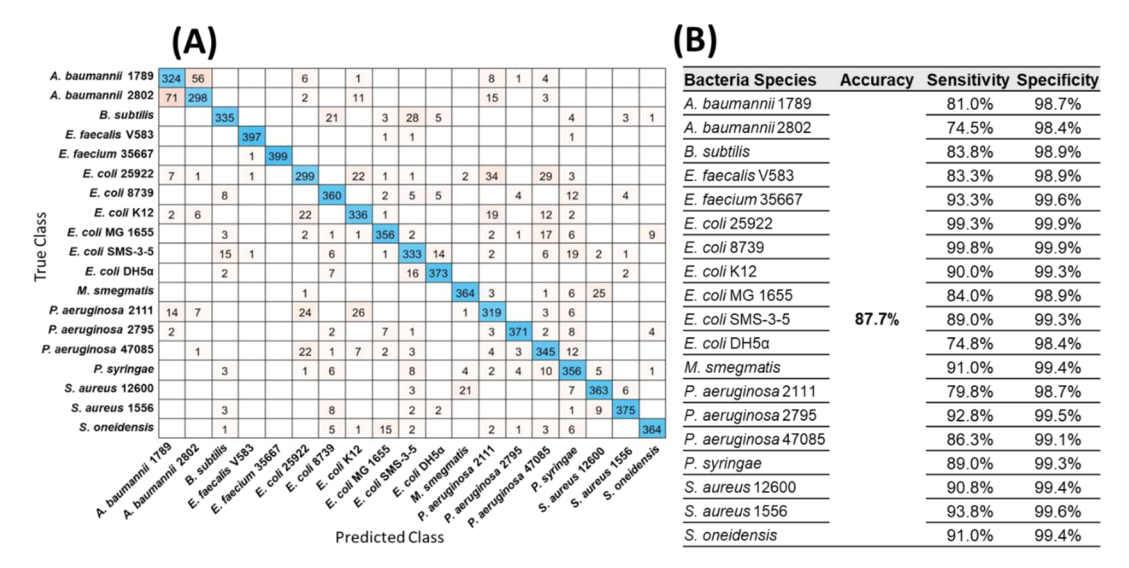


Figure 5. (A) Confusion matrix for 19 bacteria strains. The rows and columns represent the true and predictive class from a total of 400 spectra for each strain of bacteria. The diagonal entries represent the accuracies for each class (i.e., number of spectra correctly predicted from a total of 400 spectra). Entries other than the diagonal ones represent misclassifications for a given strain of bacteria. (B) Prediction results showing the overall accuracy of the SVM predictive model, sensitivity, and specificity scores for each bacteria strains calculated from the confusion matrix.

dataset (Table S3). Nonlinear SVM classifiers using the simplified computational approach of the Gaussian kernel function are quite effective as multivariate analysis tools. Previously, Kang et al. reported higher flexibility and accuracy of Gaussian kernel functions compared to discriminant analysis techniques in performing multiclass classification and nonlinear optimization. ³³

Based on 10-fold cross validation, the results for all of the bacterial strains are presented in a confusion matrix (Figure 5A). From a total of 7600 spectra, 6667 were correctly predicted and assigned to the corresponding bacteria using the model, resulting in an overall accuracy of 87.7% (Figure 5B). The predictive model showed a high sensitivity of ~89% or higher for 11 of the 19 bacterial strains. Five bacterial strains had sensitivity scores between 80 and 89%. Only two bacterial strains A. baumannii 2802 (74.5%) and E. coli Dh5 α (74.8%) had scores less than 80%. The strain, E. coli K12, was measured with five different (con A + BCNCs) substrates to account for the substrate variability on the prediction accuracy. The average accuracy from five SERS datasets of five measurements was 85.25% (Table S5), which was close to the reported accuracy of 83.5% for E. coli K12, suggesting that substrate variability had a low impact on the prediction accuracy for E. coli K12. The specificity of the model was high (\geq 98.4%) for all species (Figure 5B). Sensitivity and specificity being the correct identification of the true positives and true negatives, respectively. The high overall accuracy of 87.7% suggests that the SVM classifier performed well in discriminating the 19 bacterial strains. As the number of bacterial strains increases, the flexibility of the hyperplane for separating a large number of classes can decrease. Previously, Ho et al. observed 74.9% accuracy when using SVM to discriminate 30 bacterial strains.²⁶ Combining data-clustering methods, such as hierarchical clustering for bacterial subspecies or type strains with SVM classifiers, can be beneficial to improve the overall accuracy and sensitivity for larger datasets. 32,67 When we considered the whole spectra from 600 to 1700 cm⁻¹, the overall accuracy improved to 98.5% with nearly all spectra predicted correctly (Figure S10A,B). However, as discussed

previously, the improved accuracy obtained using a greater number of spectral features can be offset by the inclusion of spectral noise in the dataset, resulting in a potential model overfit.

CONCLUSIONS AND FUTURE OUTLOOK

In this study, we applied lectin-modified BCNCs as SERS biosensors. This approach was robust and versatile in the isolation and SERS detection of 19 bacterial strains. The tunability and biocompatibility of BCNCs allow for the hosting of guest nanoparticles and facile bioconjugation with recognition elements, such as lectins. The (con A + BCNC)based SERS substrate showed a low variability of SERS hot spots compared to many other SERS substrates, suggesting the reproducibility of the detection assay. SVM classifiers combined with the SERS detection assay proved to be a rapid and reliable method for discriminating bacterial strains with an overall accuracy of ~88%. The different techniques for SERS data preprocessing and automated feature selection processes described in the literature should be standardized for large-scale comparison of SERS datasets and better interpretation of the results from classification models, such as the SVM. Several important variables, such as varying culture conditions, substrate variability, storage conditions, time, and instrument drift can cumulatively affect the overall accuracy of different classification algorithms. It is, therefore, important to thoroughly examine the limitations posed by these variables when combining SERS datasets with machine-learning techniques. The effects of varying culture conditions on bacterial metabolite release need to be further investigated. A goal of our future work is to improve on the controlled experimental conditions in this study and apply the (con A + BCNC)-based biosensor for use in real environmental samples, where mixtures of multiple bacteria are common. Nevertheless, the advent of portable Raman systems that can potentially interface with automated machine-learning techniques holds great promise for low-cost and rapid SERS sensing in realworld environments. To maximize the benefits of combining machine-learning techniques with SERS dataset analyses, it

remains necessary to standardize SERS methodologies. This study illustrates the great potential of the application of novel BCNC-based substrates as low-cost, biocompatible, and dispersible SERS biosensors and machine learning for the discriminatory detection of bacteria. The rapid identification and discrimination of bacterial strains using this technique offer opportunities for future advancements in the development of point-of-use sensors for field deployment.

ASSOCIATED CONTENT

Supporting Information

The Supporting Information is available free of charge at https://pubs.acs.org/doi/10.1021/acsanm.1c02760.

Detailed experimental methods; characterization of nanomaterials; SERS and UV-vis spectra of con A + BCNC in the presence and absence of bacteria; SERS spectra of 19 bacterial strains; and evaluation of model accuracy (PDF)

AUTHOR INFORMATION

Corresponding Author

Peter J. Vikesland — Department of Civil and Environmental Engineering, Virginia Tech, Blacksburg, Virginia 24061, United States; Virginia Tech Institute for Critical Technology and Applied Science (ICTAS) Sustainable Nanotechnology Center (VTSuN), Blacksburg, Virginia 24061, United States; orcid.org/0000-0003-2654-5132; Phone: +1-540-231-3578; Email: pvikes@vt.edu

Authors

Asifur Rahman — Department of Civil and Environmental Engineering, Virginia Tech, Blacksburg, Virginia 24061, United States; Virginia Tech Institute for Critical Technology and Applied Science (ICTAS) Sustainable Nanotechnology Center (VTSuN), Blacksburg, Virginia 24061, United States; orcid.org/0000-0003-4889-7980

Seju Kang — Department of Civil and Environmental Engineering, Virginia Tech, Blacksburg, Virginia 24061, United States; Virginia Tech Institute for Critical Technology and Applied Science (ICTAS) Sustainable Nanotechnology Center (VTSuN), Blacksburg, Virginia 24061, United States; orcid.org/0000-0003-3281-4829

Wei Wang — Department of Civil and Environmental Engineering, Virginia Tech, Blacksburg, Virginia 24061, United States; Virginia Tech Institute for Critical Technology and Applied Science (ICTAS) Sustainable Nanotechnology Center (VTSuN), Blacksburg, Virginia 24061, United States; Occid.org/0000-0002-6231-2216

Qishen Huang — Department of Civil and Environmental Engineering, Virginia Tech, Blacksburg, Virginia 24061, United States; Virginia Tech Institute for Critical Technology and Applied Science (ICTAS) Sustainable Nanotechnology Center (VTSuN), Blacksburg, Virginia 24061, United States; orcid.org/0000-0002-8493-5799

Inyoung Kim – Department of Statistics, Virginia Tech, Blacksburg, Virginia 24061, United States

Complete contact information is available at: https://pubs.acs.org/10.1021/acsanm.1c02760

Notes

The authors declare no competing financial interest.

ACKNOWLEDGMENTS

We thank Drs. Bahareh Behkam and Eric J. Leaman at Virginia Tech for providing the two bacterial strains: *S. oneidensis* and *E. coli* MG 1655. All other bacterial strains were graciously provided by Dr. Amy Pruden. This research was supported by the National Science Foundation grant OISE-1545756. Additional support was provided by the Virginia Tech Graduate School Sustainable Nanotechnology (VTSuN) program. Instrumental access was provided through the NanoEarth node of the NSF NNCI (Award 2025151).

REFERENCES

- (1) Vikesland, P. J.; Pruden, A.; Alvarez, P. J. J.; Aga, D.; Bürgmann, H.; Li, X. D.; Manaia, C. M.; Nambi, I.; Wigginton, K.; Zhang, T.; Zhu, Y. G. Toward a Comprehensive Strategy to Mitigate Dissemination of Environmental Sources of Antibiotic Resistance. *Environ. Sci. Technol.* **2017**, *51*, 13061–13069.
- (2) Vikesland, P. J. Nanosensors for water quality monitoring. *Nat. Nanotechnol.* **2018**, *13*, 651–660.
- (3) Wang, Y.; Ravindranath, S.; Irudayaraj, J. Separation and detection of multiple pathogens in a food matrix by magnetic SERS nanoprobes. *Anal. Bioanal. Chem.* **2011**, 399, 1271–1278.
- (4) Kearns, H.; Goodacre, R.; Jamieson, L. E.; Graham, D.; Faulds, K. SERS Detection of Multiple Antimicrobial-Resistant Pathogens Using Nanosensors. *Anal. Chem.* **2017**, *89*, 12666–12673.
- (5) Langer, J.; Jimenez de Aberasturi, D.; Aizpurua, J.; Alvarez-Puebla, R. A.; Auguié, B.; Baumberg, J. J.; Bazan, G. C.; Bell, S. E. J.; Boisen, A.; Brolo, A. G.; Choo, J.; Cialla-May, D.; Deckert, V.; Fabris, L.; Faulds, K.; García de Abajo, F. J.; Goodacre, R.; Graham, D.; Haes, A. J.; Haynes, C. L.; Huck, C.; Itoh, T.; Käll, M.; Kneipp, J.; Kotov, N. A.; Kuang, H.; le Ru, E. C.; Lee, H. K.; Li, J.-F.; Ling, X. Y.; Maier, S.; Mayerhöfer, T.; Moskovits, M.; Murakoshi, K.; Nam, J.-M.; Nie, S.; Ozaki, Y.; Pastoriza-Santos, I.; Perez-Juste, J.; Popp, J.; Pucci, A.; Reich, S.; Ren, B.; Schatz, G. C.; Shegai, T.; Schlücker, S.; Tay, L. L.; Thomas, K. G.; Tian, Z.-Q.; van Duyne, R. P.; Vo-Dinh, T.; Wang, Y.; Willets, K. A.; Xu, C.; Xu, H.; Xu, Y.; Yamamoto, Y. S.; Zhao, B.; Liz-Marzán, L. M. Present and Future of Surface-Enhanced Raman Scattering. ACS Nano 2020, 14, 28–117.
- (6) Wei, H.; Leng, W.; Song, J.; Willner, M. R.; Marr, L. C.; Zhou, W.; Vikesland, P. J. Improved Quantitative SERS Enabled by Surface Plasmon Enhanced Elastic Light Scattering. *Anal. Chem.* **2018**, *90*, 3227–3237.
- (7) Fan, M. K.; Brolo, A. G. Silver nanoparticles self assembly as SERS substrates with near single molecule detection limit. *Phys. Chem. Chem. Phys.* **2009**, *11*, 7381–7389.
- (8) Lenzi, E.; Jimenez de Aberasturi, D.; Liz-Marzán, L. M. Surface-Enhanced Raman Scattering Tags for Three-Dimensional Bioimaging and Biomarker Detection. *ACS Sens.* **2019**, *4*, 1126–1137.
- (9) Alafeef, M.; Moitra, P.; Pan, D. Nano-enabled sensing approaches for pathogenic bacterial detection. *Biosens. Bioelectron.* **2020**, *165*, No. 112276.
- (10) Wang, J.; Wu, X.; Wang, C.; Rong, Z.; Ding, H.; Li, H.; Li, S.; Shao, N.; Dong, P.; Xiao, R.; Wang, S. Facile Synthesis of Au-Coated Magnetic Nanoparticles and Their Application in Bacteria Detection via a SERS Method. *ACS Appl. Mater. Interfaces* **2016**, *8*, 19958–19967.
- (11) Tadesse, L. F.; Ho, C.-S.; Chen, D.-H.; Arami, H.; Banaei, N.; Gambhir, S. S.; Jeffrey, S. S.; Saleh, A. A.; Dionne, J. Plasmonic and Electrostatic Interactions Enable Uniformly Enhanced Liquid Bacterial Surface-Enhanced Raman Scattering (SERS). *Nano Lett.* **2020**, *20*, 7655–7661.
- (12) Wei, H.; Rodriguez, K.; Renneckar, S.; Vikesland, P. J. Environmental science and engineering applications of nanocellulose-based nanocomposites. *Environ. Sci.: Nano* **2014**, *1*, 302–316.
- (13) Chen, R.; Zhang, L.; Li, X.; Ong, L.; Soe, Y. G.; Sinsua, N.; Gras, S. L.; Tabor, R. F.; Wang, X.; Shen, W. Trace Analysis and Chemical Identification on Cellulose Nanofibers-Textured SERS

- Substrates Using the "Coffee Ring" Effect. ACS Sens. 2017, 2, 1060–1067.
- (14) Wei, H.; Rodriguez, K.; Renneckar, S.; Leng, W.; Vikesland, P. J. Preparation and evaluation of nanocellulose—gold nanoparticle nanocomposites for SERS applications. *Analyst* **2015**, *140*, 5640—5649.
- (15) Kang, S.; Rahman, A.; Boeding, E.; Vikesland, P. J. Synthesis and SERS application of gold and iron oxide functionalized bacterial cellulose nanocrystals (Au@Fe₃O₄@BCNCs). *Analyst* **2020**, *145*, 4358–4368.
- (16) Ogundare, S. A.; van Zyl, W. E. A review of cellulose-based substrates for SERS: fundamentals, design principles, applications. *Cellulose* **2019**, *26*, 6489–6528.
- (17) Zhang, L.; Li, X.; Ong, L.; Tabor, R. F.; Bowen, B. A.; Fernando, A. I.; Nilghaz, A.; Garnier, G.; Gras, S. L.; Wang, X. G.; Shen, W. Cellulose nanofibre textured SERS substrate. *Colloids Surf.*, A 2015, 468, 309–314.
- (18) He, H.; Chen, R.; Zhang, L.; Shen, W. Growth of gold nanoparticles on cellulose nanofibers. *Cellulose* **2020**, *27*, 5041–5053.
- (19) Bossa, N.; Carpenter, A. W.; Kumar, N.; de Lannoy, C.-F.; Wiesner, M. Cellulose nanocrystal zero-valent iron nanocomposites for groundwater remediation. *Environ. Sci.: Nano* **2017**, *4*, 1294–1303
- (20) Brinkmann, A.; Chen, M.; Couillard, M.; Jakubek, Z. J.; Leng, T.; Johnston, L. J. Correlating Cellulose Nanocrystal Particle Size and Surface Area. *Langmuir* **2016**, 32, 6105–6114.
- (21) Hirabayashi, J. Concept, Strategy and Realization of Lectin-based Glycan Profiling. *J. Biochem.* **2008**, *144*, 139–147.
- (22) Gao, J.; Liu, D.; Wang, Z. Screening Lectin-Binding Specificity of Bacterium by Lectin Microarray with Gold Nanoparticle Probes. *Anal. Chem.* **2010**, 82, 9240–9247.
- (23) Willner, M. R.; McMillan, K. S.; Graham, D.; Vikesland, P. J.; Zagnoni, M. Surface-Enhanced Raman Scattering Based Microfluidics for Single-Cell Analysis. *Anal. Chem.* **2018**, *90*, 12004–12010.
- (24) Mi, F.; Guan, M.; Hu, C.; Peng, F.; Sun, S.; Wang, X. Application of lectin-based biosensor technology in the detection of foodborne pathogenic bacteria: a review. *Analyst* **2021**, *146*, 429–443.
- (25) Lussier, F.; Thibault, V.; Charron, B.; Wallace, G. Q.; Masson, J.-F. Deep learning and artificial intelligence methods for Raman and surface-enhanced Raman scattering. *TrAC-Trends Anal. Chem.* **2020**, 124, No. 115796.
- (26) Ho, C.-S.; Jean, N.; Hogan, C. A.; Blackmon, L.; Jeffrey, S. S.; Holodniy, M.; Banaei, N.; Saleh, A. A.; Ermon, S.; Dionne, J. Rapid identification of pathogenic bacteria using Raman spectroscopy and deep learning. *Nat. Commun.* **2019**, *10*, 4927.
- (27) Thrift, W. J.; Cabuslay, A.; Laird, A. B.; Ranjbar, S.; Hochbaum, A. I.; Ragan, R. Surface-Enhanced Raman Scattering-Based Odor Compass: Locating Multiple Chemical Sources and Pathogens. *ACS Sens.* **2019**, *4*, 2311–2319.
- (28) Thrift, W. J.; Ronaghi, S.; Samad, M.; Wei, H.; Nguyen, D. G.; Cabuslay, A. S.; Groome, C. E.; Santiago, P. J.; Baldi, P.; Hochbaum, A. I.; Ragan, R. Deep Learning Analysis of Vibrational Spectra of Bacterial Lysate for Rapid Antimicrobial Susceptibility Testing. *ACS Nano* 2020, *14*, 15336–15348.
- (29) Noble, W. S. What is a support vector machine? *Nat. Biotechnol.* **2006**, 24, 1565–1567.
- (30) Cristianini, N.; Shawe-Taylor, J. Support Vector Machines and other kernel-based learning methods; Cambridge University Press, 2004.
- (31) Pisner, D. A.; Schnyer, D. M. Support vector machine. In Machine Learning; Academic Press, 2020, pp. 101–121.
- (32) Kusić, D.; Kampe, B.; Rösch, P.; Popp, J. Identification of water pathogens by Raman microspectroscopy. *Water Res.* **2014**, *48*, 179–189.
- (33) Kang, S.; Kim, I.; Vikesland, P. J. Discriminatory detection of ssDNA by surface-enhanced Raman spectroscopy (SERS) and tree-based support vector machines (Tr-SVM). *Anal. Chem.* **2021**, *93*, 9319–9328.

- (34) Brown, K. R.; Walter, D. G.; Natan, M. Seeding of Colloidal Au Nanoparticle Solutions. 2. Improved Control of Particle Size and Shape. *J. Chem. Mater.* **2000**, *12*, 306–313.
- (35) Saito, T.; Hirota, M.; Tamura, N.; Kimura, S.; Fukuzumi, H.; Heux, L.; Isogai, A. Individualization of Nano-Sized Plant Cellulose Fibrils by Direct Surface Carboxylation Using TEMPO Catalyst under Neutral Conditions. *Biomacromolecules* **2009**, *10*, 1992–1996.
- (36) Nakajima, N.; Ikada, Y. Mechanism of amide formation by carbodiimide for bioconjugation in aqueous media. *Bioconjugate Chem.* **1995**, *6*, 123–130.
- (37) Zheng, M.; Davidson, F.; Huang, X. Y. Ethylene Glycol Monolayer Protected Nanoparticles for Eliminating Nonspecific Binding with Biological Molecules. *J. Am. Chem. Soc.* **2003**, *125*, 7790–7791.
- (38) Cui, L.; Zhang, D.; Yang, K.; Zhang, X.; Zhu, Y.-G. Perspective on Surface-Enhanced Raman Spectroscopic Investigation of Microbial World. *Anal. Chem.* **2019**, *91*, 15345–15354.
- (39) Chisanga, M.; Muhamadali, H.; Ellis, D. I.; Goodacre, R. Rapid differentiation of *Campylobacter jejuni* cell wall mutants using Raman spectroscopy, SERS and mass spectrometry combined with chemometrics. *Appl. Spectrosc.* **2018**, *72*, 987–1000.
- (40) Varpa, K.; Joutsijoki, H.; Iltanen, K.; Juhola, M. Applying onevs-one and one-vs-all classifiers in k-nearest neighbour method and support vector machines to an otoneurological multi-class problem. Stud. Health Technol. Inform. 2011, 169, 579–583.
- (41) Firon, N.; Ofek, I.; Sharon, N. Carbohydrate-binding sites of the mannose-specific fimbrial lectins of enterobacteria. *Infect. Immun.* **1984**, *43*, 1088–1090.
- (42) Rusin, C. J.; El Bakkari, M.; Du, R.; Boluk, Y.; McDermott, M. T. Plasmonic Cellulose Nanofibers as Water-Dispersible Surface-Enhanced Raman Scattering Substrates. *ACS Appl. Nano Mater.* **2020**, 3, 6584–6597.
- (43) Islam, M.; Chen, L.; Sisler, J.; Tam, K. Cellulose nanocrystal (CNC)—inorganic hybrid systems: synthesis, properties and applications. *J. Mater. Chem. B* **2018**, *6*, 864—883.
- (44) Wei, H.; McCarthy, A.; Song, J.; Zhou, W.; Vikesland, P. J. Quantitative SERS by hot spot normalization surface enhanced Rayleigh band intensity as an alternative evaluation parameter for SERS substrate performance. *Faraday Discuss.* **2017**, 205, 491–504.
- (45) Wei, H.; Leng, W.; Song, J.; Liu, C.; Willner, M. R.; Huang, Q.; Zhou, W.; Vikesland, P. J. Real-Time Monitoring of Ligand Exchange Kinetics on Gold Nanoparticle Surfaces Enabled by Hot Spot-Normalized Surface-Enhanced Raman Scattering. *Environ. Sci. Technol.* **2019**, *53*, 575–585.
- (46) Wei, H.; Huang, Q.; Vikesland, P. J. The Aromatic Amine pKa Determines the Affinity for Citrate-Coated Gold Nanoparticles: In Situ Observation via Hot Spot-Normalized Surface-Enhanced Raman Spectroscopy. *Environ. Sci. Technol. Lett.* **2019**, *6*, 199–204.
- (47) Betz, J. F.; Cheng, Y.; Rubloff, G. W. Direct SERS detection of contaminants in a complex mixture: rapid, single step screening for melamine in liquid infant formula. *Analyst* **2012**, *137*, 826–828.
- (48) Weiss, R.; Palatinszky, M.; Wagner, M.; Niessner, R.; Elsner, M.; Seidel, M.; Ivleva, N. P. Surface-enhanced Raman spectroscopy of microorganisms: limitations and applicability on the single-cell level. *Analyst* **2019**, *144*, 943–953.
- (49) Chisanga, M.; Muhamadali, H.; Kimber, R.; Goodacre, R. Quantitative detection of isotopically enriched E. coli cells by SERS. *Faraday Discuss.* **2017**, 205, 331–343.
- (50) Sengupta, A.; Laucks, M. L.; Davis, E. J. Surface-Enhanced Raman Spectroscopy of Bacteria and Pollen. *Appl. Spectrosc.* **2005**, *59*, 1016–1023.
- (51) García-Timermans, C.; Rubbens, P.; Kerckhof, F.-M.; Buysschaert, B.; Khalenkow, D.; Waegeman, W.; Skirtach, A. G.; Boon, N. Label-free Raman characterization of bacteria calls for standardized procedures. *J. Microbiol. Methods* **2018**, *151*, 69–75.
- (52) Premasiri, W. R.; Gebregziabher, Y.; Ziegler, L. D. On the Difference between Surface-Enhanced Raman Scattering (SERS) Spectra of Cell Growth Media and Whole Bacterial Cells. *Appl. Spectrosc.* **2011**, *65*, 493–499.

- (53) Kahraman, M.; Keseroğlu, K.; Çulha, M. On Sample Preparation for Surface-Enhanced Raman Scattering (SERS) of Bacteria and the Source of Spectral Features of the Spectra. *Appl. Spectrosc.* **2011**, *65*, 500–506.
- (54) Muhamadali, H.; Chisanga, M.; Subaihi, A.; Goodacre, R. Combining Raman and FT-IR Spectroscopy with Quantitative Isotopic Labeling for Differentiation of E. coli Cells at Community and Single Cell Levels. *Anal. Chem.* **2015**, *87*, 4578–4586.
- (55) Walter, A.; März, A.; Schumacher, W.; Rösch, P.; Popp, J. Towards a fast, high specific and reliable discrimination of bacteria on strain level by means of SERS in a microfluidic device. *Lab Chip* **2011**, *11*, 1013–1021.
- (56) Harz, M.; Rösch, P.; Peschke, K.-D.; Ronneberger, O.; Burkhardt, H.; Popp, J. Micro-Raman spectroscopic identification of bacterial cells of the genus *Staphylococcus* and dependence on their cultivation conditions. *Analyst* **2005**, *130*, 1543–1550.
- (57) Morelli, L.; Andreasen, S. Z.; Jendresen, C. B.; Nielsen, A. T.; Emnéus, J.; Zór, K.; Boisen, A. Quantification of a bacterial secondary metabolite by SERS combined with SLM extraction for bioprocess monitoring. *Analyst* **2017**, *142*, 4553–4559.
- (58) Andreasen, S. Z.; Sanger, K.; Jendresen, C. B.; Nielsen, A. T.; Emnéus, J.; Boisen, A.; Zór, K. Extraction, Enrichment, and in situ Electrochemical Detection on Lab-on-a-Disc: Monitoring the Production of a Bacterial Secondary Metabolite. *ACS Sens.* **2019**, *4*, 398–405.
- (59) Simoska, O.; Sans, M.; Fitzpatrick, M. D.; Crittenden, C. M.; Eberlin, L. S.; Shear, J. B.; Stevenson, K. J. Real-Time Electrochemical Detection of Pseudomonas aeruginosa Phenazine Metabolites Using Transparent Carbon Ultramicroelectrode Arrays. *ACS Sens.* **2019**, *4*, 170–179.
- (60) de Marchi, S.; Bodelón, G.; Vázquez-Iglesias, L.; Liz-Marzán, L. M.; Pérez-Juste, J.; Pastoriza-Santos, I. Surface-enhanced Raman scattering (SERS) imaging of bioactive metabolites in mixed bacterial populations. *Appl. Mater. Today* **2019**, *14*, 207–215.
- (61) Wichmann, C.; Chhallani, M.; Bocklitz, T.; Rösch, P.; Popp, J. Simulation of transportation and storage and their influence on Raman spectra of bacteria. *Anal. Chem.* **2019**, *91*, 13688–13694.
- (62) Chen, L.; Mungroo, N.; Daikuara, L.; Neethirajan, S. Label-free NIR-SERS discrimination and detection of foodborne bacteria by in situ synthesis of Ag colloids. *J. Nanobiotechnol.* **2015**, *13*, 45.
- (63) Hoehse, M.; Paul, A.; Gornushkin, I.; Panne, U. Multivariate classification of pigments and inks using combined Raman spectroscopy and LIBS. *Anal. Bioanal. Chem.* **2012**, 402, 1443–1450.
- (64) Xu, Y.; Zomer, S.; Brereton, R. G. Support Vector Machines: A Recent Method for Classification in Chemometrics. *Crit. Rev. Anal. Chem.* **2006**, *36*, 177–188.
- (65) Fereiduni, E.; Ghasemi, A.; Elbestawi, M. Characterization of Composite Powder Feedstock from Powder Bed Fusion Additive Manufacturing Perspective. *Materials* **2019**, *12*, 3673.
- (66) Seeger, M. Gaussian processes for machine learning. *Int. J. Neural Syst.* **2004**, *14*, 69–106.
- (67) Kung, H.-C.; Chen, R.-M.; Tsai, J. J.; Hu, R.-M. Stratification of Human Gut Microbiome and Building a SVM-Based Classifier. In *The 18th International Conference on Bioinformatics and Bioengineering* (BIBE); IEEE: China, 29–31 Oct. 2018.

□ Recommended by ACS

Simultaneous Optical Detection of Multiple Bacterial Species Using Nanometer-Scaled Metal-Organic Hybrids

So Tanabe, Hiroshi Shiigi, et al.

JULY 25, 2022

ANALYTICAL CHEMISTRY

READ 🗹

Delineating the Role of Tailored Gold Nanostructures at the Biointerface

Adarsh P. Fatrekar, Amit A. Vernekar, et al.

NOVEMBER 30, 2021

ACS APPLIED BIO MATERIALS

READ 🗹

Development and Validation of a SERS-Based Serological Test Combined with PLS-DA Method for Leishmaniasis Detection

Rodrigo S. N. Mancini, Wendel A. Alves, et al.

AUGUST 10, 2022

ACS APPLIED ELECTRONIC MATERIALS

READ 🗹

Single-Walled Carbon Nanotube Probes for the Characterization of Biofilm-Degrading Enzymes Demonstrated against *Pseudomonas aeruginosa* Extracell...

Sparsh Agarwal, Nigel F. Reuel, et al.

DECEMBER 23, 2021

ANALYTICAL CHEMISTRY

READ 🗹

Get More Suggestions >